Experimental simulation of subsurface crack formation in continuous casting*

C. Bernhard, H. Hiebler, M.M. Wolf
(Montanuniversität Leoben, Austria)

With increasing casting speed or/and the addition of B, P or S as microalloying elements, assurance of crack-free products becomes more difficult. A new laboratory test method is developed which allows to study crack formation under conditions closely simulating the solidification in the continuous casting mould. Pertinent results and their potential application to CC process control are described in the paper.

■ INTRODUCTION

The trend to ever increasing casting speeds and, concurrently, the higher crack susceptibility of steels with additions of boron, phosphorus or sulphur endangers the inner soundness of continuously cast (CC) products. The example of *figure 1* illustrates severe inner crack formation of a low carbon (LC) steel with low Mn/S ratio (1). Such form of macrosegregation persists throughout further processing, leading to a "banded" microstructure or/and enhanced grain boundary segregation which may impair final product properties, e.g. the phenomenon of "cold work embrittlement" (CWE) of rephosphorized ultra-low carbon (ULC) steels (2) (3) (4).

Subsurface cracks are a particularly dangerous inner defect, since they also can cause surface cracks and breakouts (BO). Apart from frequent occurrence in the midface region (within the "shadow" of the submerged entry nozzle, SEN), the offcorner position is mostly affected *(fig. 1)* where tensile stress prevails and crack hazard is increasing at higher P- or S-content according to the analysis by Wintz et al. (5). This is confirmed in plant observations on subsurface off-corner cracking in bloom casting of engineering steels (6), for instance, with the following main characteristics derived from *figure 2* :

- maximum crack susceptibility at medium carbon content of 0.3-0.4 % C ;
- enhanced crack incidence with reduced Mn/S ratio ;
- reduced cracking by increasing the mould taper.

The latter effect of mould geometry has been attributed in extensive work by the late Professor J.K. Brimacombe and associates to the balance between shell contraction and face bulging which may lead to corner "rotation" and, hence, to reduced heat transfer in the off-corner position where a surface depression with a "hot spot" is formed (7) (8) *(fig. 3)* ; such detrimental behaviour being much favoured by the commonly applied linear mould taper (9). In one quantitative analysis for slab casting (10) *(fig. 4)*, it is shown that, instead of continuous cooling, the surface reheats from about 1250 to over 1300 °C at a position 25 mm from the corner in case of a modest narrow face (NF) taper of 0.9 %/m, but reheating is eliminated by increasing the taper to 1.4 %/m – in favour of improved BO safety. The relevance of such studies is highlighted for the particularly critical situation of slab "widening", i.e. width increase during casting (11).

* *Subject of a presentation at the 1999 ATS International Steelmaking Conference (Paris, December 8-9, 1999, Session 2).*

Simulation expérimentale de la formation des criques sous-cutanées en coulée continue

C. Bernhard, H. Hiebler, M.M. Wolf
(Montanuniversität Leoben, Autriche)

Les exigences de productivité en coulée continue, ainsi que l'élaboration d'aciers propres à hautes caractéristiques, c'est-à-dire contenant du B, P et/ou S en teneurs contrôlées, peuvent entraîner des problèmes de santé interne. Un de ces phénomènes nocifs est la formation de criques d'angle qui peuvent même causer des percées. Normalement, ces criques sont sous-cutanées et se trouvent à l'aplomb de dépressions superficielles. Elles se manifestent par des « taches chaudes », visibles à la surface du produit coulé. Une des mesures courantes pour les éviter est l'augmentation de la conicité de la lingotière.

Méthode de simulation

Afin de mieux connaître l'effet de la nuance, on a développé une méthode de simulation de la peau en lingotière appelée essai SSCT. On utilise un dispositif en deux parties qui est immergé dans le bain de métal ; après un temps de séjour de plusieurs secondes nécessaires pour créer une première peau, une force hydraulique est appliquée pour séparer les deux parties du dispositif et exercer ainsi une traction sur la peau solidifiée. Pour un allongement de la peau compris entre 1,6 et 4,0 %, la vitesse d'allongement est d'environ 0,3-0,8 %/s, ce qui est très représentatif des conditions en coulée continue. En faisant varier le revêtement du dispositif, on obtient différentes vitesses de refroidissement correspondant à des flux thermiques extraits compris entre 1,5 et 6,0 MW par m^2. Au cours de l'essai, une analyse thermique suit la croissance de la peau, et le modèle de microségregation de Ohnaka permet de caractériser le métal solidifié.

Résultats

Les résultats obtenus dans le cas des nuances à haute teneur en carbone montrent qu'il existe un domaine critique de température (CTR = critical temperature range) dans lequel il y a formation de criques interdendritiques : c'est le domaine dans lequel le rapport T/T_S (température absolue de la peau/température absolue de solidification) est compris entre 0,8 et 1,0. Dans les aciers à 0,6 % C, le seuil d'apparition de criques se situe à T/T_S égal à 0,90, ce qui correspond à une contrainte de rupture de la peau de 5 MPa et un allongement de 1,6 %. La nuance à 0,2 % de carbone et une addition de bore se fissure quelles que soient les conditions d'essai (notamment pour un allongement de 3,6 %). Les nuances à bas carbone ne se fissurent que pour un rapport T/T_S supérieur à 0,95, ce qui correspond à une résistance critique inférieure à 2 MPa.

Interprétation

D'après les essais réalisés, la structure de solidification elle-même ne joue pas un rôle fondamental. Il n'y a pas grande différence de comportement entre les dendrites à croissance cellulaire que l'on rencontre dans les aciers à bas carbone et les dendrites à larges bras ramifiés que possèdent les aciers à haut carbone. La criquabilité semble plutôt liée à la présence ou non de précipités interdendritiques ou intergranulaires. Pour confirmer ce mécanisme, il faudrait déterminer la concentration en impuretés des zones interdendriques ségrégées.

Application à la conduite des machines de coulée continue

Le fait de connaître la résistance mécanique de la peau solidifiée aux températures proches du solidus et le rôle primordial de la température relative (T/T_S) de la surface permet, sans nécessairement connaître le mécanisme, de mieux maîtriser le processus de solidification en lingotière. Pour cela, il faut équiper la lingotière de thermocouples disposés en paroi et se servir de leurs indications pour apprécier le risque de formation de criques sous-cutanées.

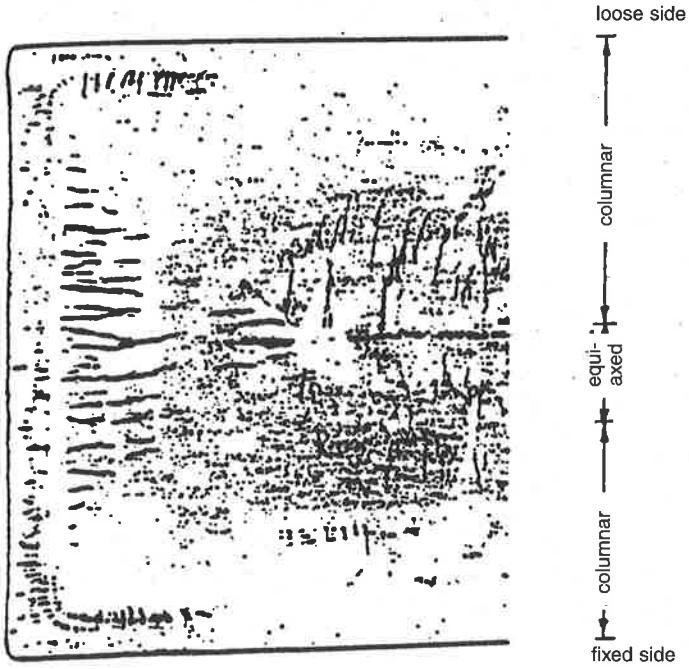

Fig. 1 – Example of inner cracks in slab casting with Mn/S ratio of 4.9 (1). Steel analysis (wt-%) : 0.04 C, 0.01 Si, 0.27 Mn, 0.022 P, 0.055 S, 0.040 Al.

Fig. 1 – Exemple de criques internes en coulée continue de brames avec rapport Mn/S de 4.9 (1).

Obviously, for each case there exists a critical strand surface temperature, T_0 which – for a given level of tensile stress – relates to the limit of local shell strength, σ_B. Pertinent data are still scarce but can conveniently be obtained from the new simulation method, termed "Submerged Split Chill Tensile" (SSCT) test (12 to 14). This method offers the following characteristic features :

- testing is performed in-situ during solidification and perpendicular to the main dendrite growth axis in order to reveal the effect of interdendritic and intergranular precipitates on cohesive strength under conditions closely simulating the CC process ;
- low strain rate testing is applied, i.e. about 0.1-1.0 %/s, again close to CC conditions ;
- cooling rates can be adjusted within a wide range, with heat flux intensities between 1.5 and 6.0 MW/m^2 to simulate various CC technologies, e.g. mould lubrication by oil or powder.

In the following, an investigation pertaining to subsurface cracking under simulated CC conditions is presented for a variety of C-steels.

■ EXPERIMENTAL CONDITIONS

The SSCT test method is schematically presented in *figure 5*. A solid steel test body, split in two halves, is submerged into the melt contained in an induction furnace. During the initial holding time (6 to 14 s), a steel shell solidifies around the test body. The cooling intensity is controlled by refractory coatings on the test body, and the progress of solidification monitored via thermocouples.

At the end of holding time (2-14 s), the lower half of the test body is moved downward by hydraulic force. Force and elongation are recorded and converted into stress-strain curves (see example in *figure 6*). Usually, a strain of maxi-

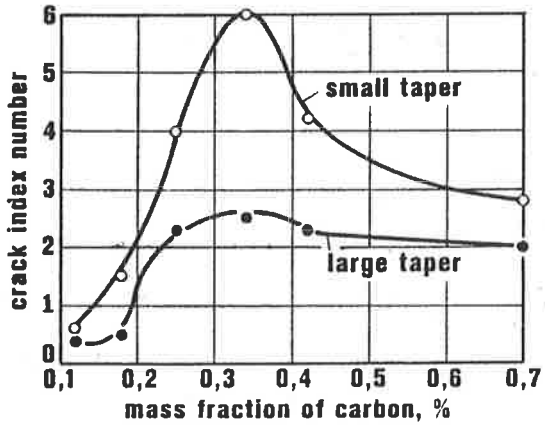

a)

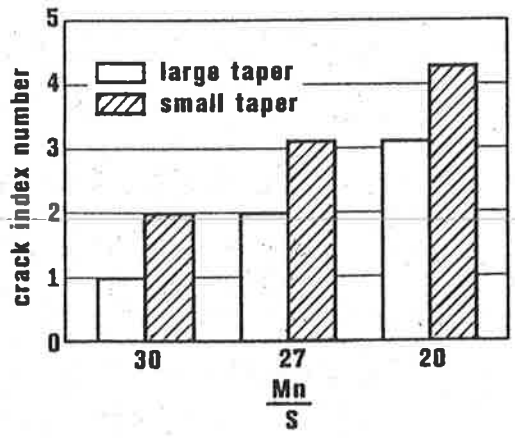

b)

Fig. 2 – Dependence of subsurface off-corner cracks in special steel bloom casting on (a) C-content, and on (b) Mn/S ratio as well as mould taper (6).

Fig. 2 – Criques d'angles sous-cutanées en coulée continue des blooms en aciers spéciaux affectées par (a) la teneur en carbone et (b) le rapport Mn/S, ainsi que la conicité de la lingotière (6).

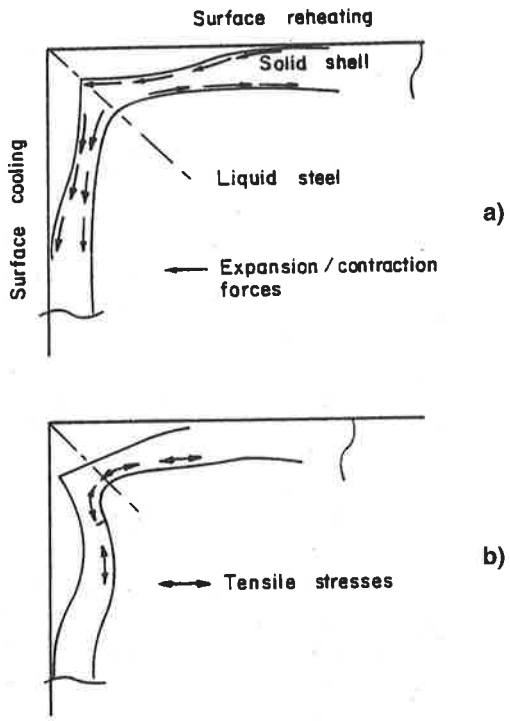

Fig. 3 – Schematic for (a) corner gap formation, and (b) corner rotation, leading to subsurface off-corner crack formation (8).

Fig. 3 – Présentation schématique de (a) la formation d'un décollement aux angles, et (b) la rotation des coins entraînant la formation de criques sous-cutanées près des angles (8).

mum 1.6-4.0 %, i.e. 0.8-2.0 mm over the 50 mm test length, is applied. With loading times of around 5 s, average strain rates of 0.3-0.8 %/s (= $3\text{-}8 \cdot 10^{-3}$ s^{-1}) are realized. The simultaneous thermal analysis yields the temperature distribution in the steel shell over time *(fig. 7)*. T_S' is the solidus temperature derived by microsegregation modelling according to Ohnaka (15) ; other characteristic temperatures are the bulk temperature of the shell (T_B) and the shell surface temperature (T_0). After tensile testing, test body and steel shell are immediately withdrawn from the melt. Steel shells are subjected to metallographic examination (i.e. Béchet-Beaujard etching for dendritic structure), and characteristic features evaluated such as dendrite spacing, crack occurrence, and also concentration mapping by microanalyser.

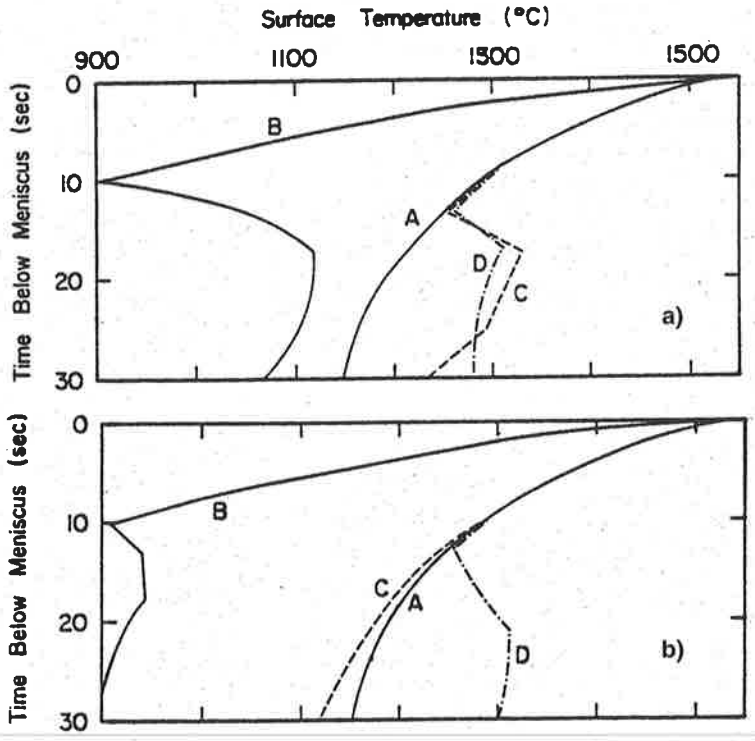

Fig. 4 – Slab surface temperature profiles (220 × 1100 mm² ; 1.2 m/min) for two mould tapers : (a) 0.9 and (b) 1.4 %/m (10).
A : midface (narrow and wide) ; B : slab corner ; C : at 25 mm from corner at NF ; D : at 25 mm from corner at WF.

Fig. 4 – Profils de température en surface de brame (220 × 1100 mm² ; 1.2 m/min) pour deux conicités en lingotière : (a) 0,9 et (b) 1,4 %/m (10).
A : mi-face (petite et grande) ; B : angle de brame ; C : à 25 mm de l'angle sur petite face ; D : à 25 mm de l'angle sur la grande face.

■ TEST RESULTS

As apparent from the lower curve in *figure 6*, a distinct peak stress, σ_p is often attained (here at the strain of 0.4 %) ; the subsequent stress decay is attributed to shell weakening on account of interdendritic or/and intergranular cracking. Such crack formation is shown by the two examples in *figures 8 and 9* for steel types C60 and C20B respectively. According to the thermal analysis, crack extension clearly coincides with the position for the isotherms of $f_S \sim 0.8\text{-}1.0$ which is commonly considered as the "Critical Temperature Range" (CTR) for inner crack formation, e.g. (5) (16).

A summary for all test results with C60 and C20B type steel samples concerning inner crack occurrence is given in *figures 10 and 11*. Taking the homologous temperature, T_0/T_S' as essential criterion for shell strength near the melting point, the following observations can be derived :

- for C60 steels, a maximum homologous temperature of 0.90 ($T_0 < 1238$ °C) is permissible to prevent major crack incidences (for strain of 1.6 %) ;
- for C20B steels, no crack free samples were found within the applied test range of T_0/T_S' greater than 0.80 (for strain of about 3.6 %), but the advantage of lower homologous (or surface) temperature is obvious as far as shell decohesion resistance is concerned.

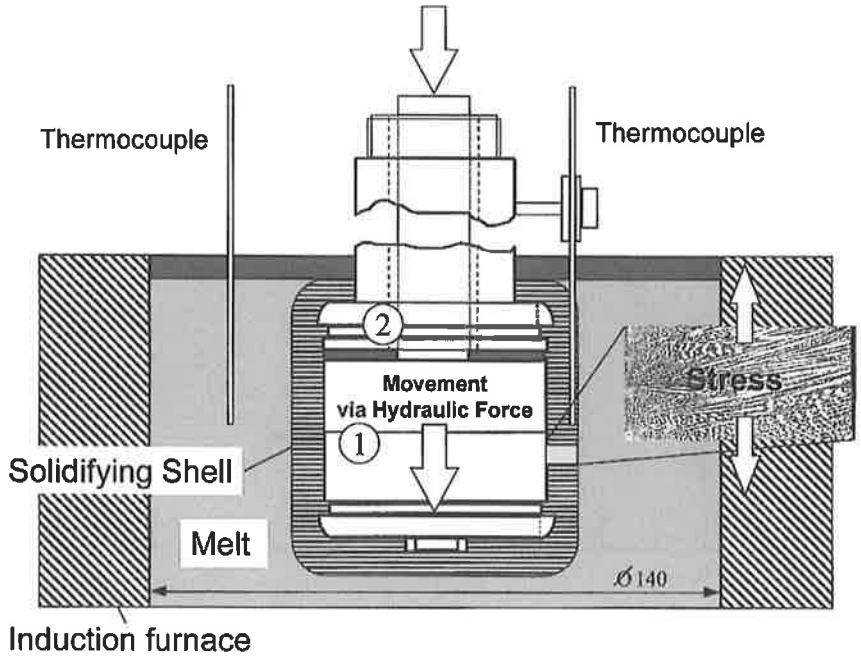

Fig. 5 – Schematic presentation of the SSCT test method, position of thermocouples and geometry of chill body.

Fig. 5 – Présentation schématique de l'essai SSCT, position des thermocouples et géométrie du dispositif de refroidissement.

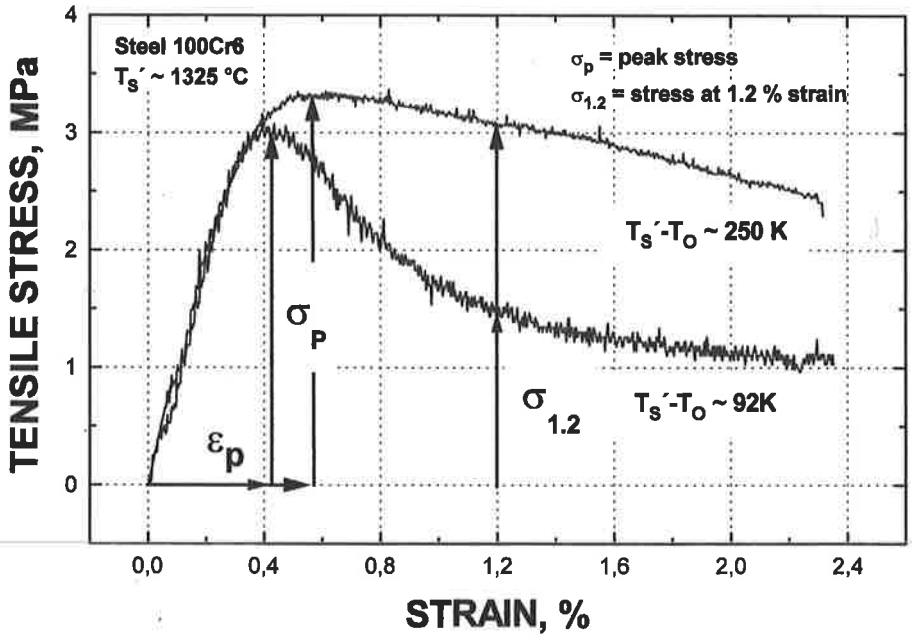

Fig. 6 – Example of stress-strain curve in the SSCT test obtained for steel 100Cr6 and two cooling intensities.

Fig. 6 – Exemple d'une courbe contrainte-allongement en essai SSCT obtenu pour un acier 100Cr6 et deux intensités de refroidissement.

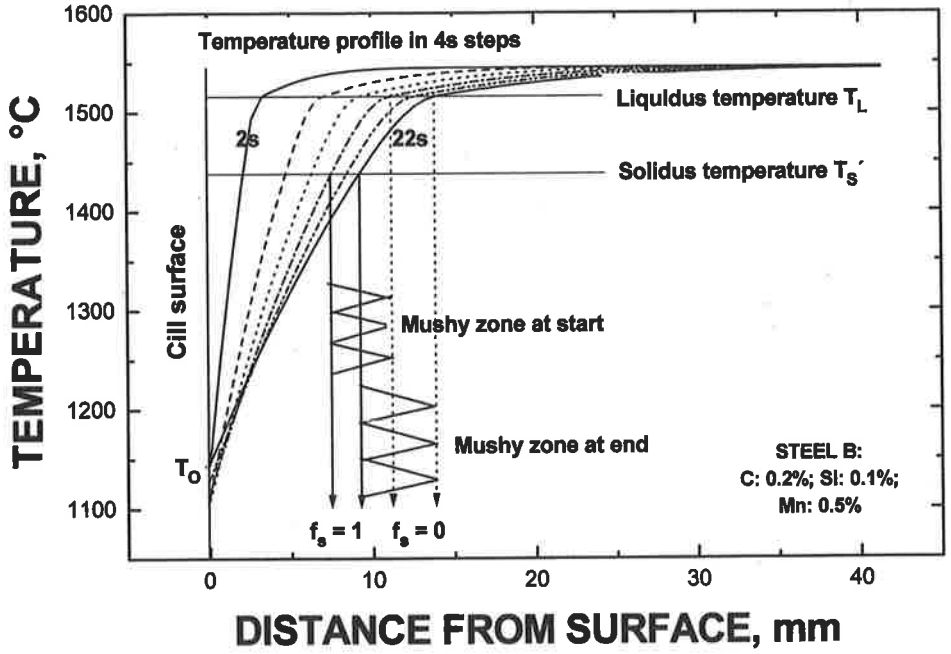

Fig. 7 – Thermal analysis during SSCT test, schematic.

Fig. 7 – Analyse thermique pendant l'essai SSCT (schéma).

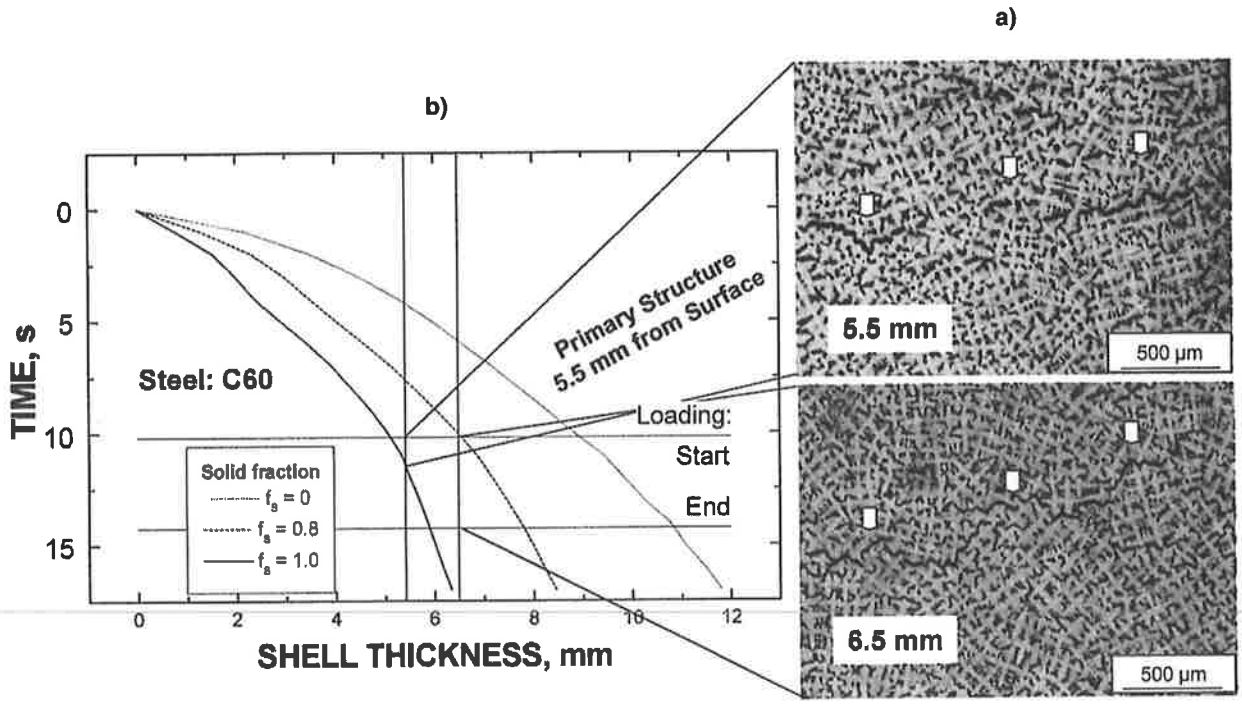

Fig. 8 – Microsection with interdendritic crack (a) and shell growth derived from thermal analysis during SSCT test (b) for steel C60.

Fig. 8 – Section métallographique avec crique interdendritique (a) et croissance de peau calculée à partir de l'analyse thermique pendent l'essai SSCT (b) pour acier C60.

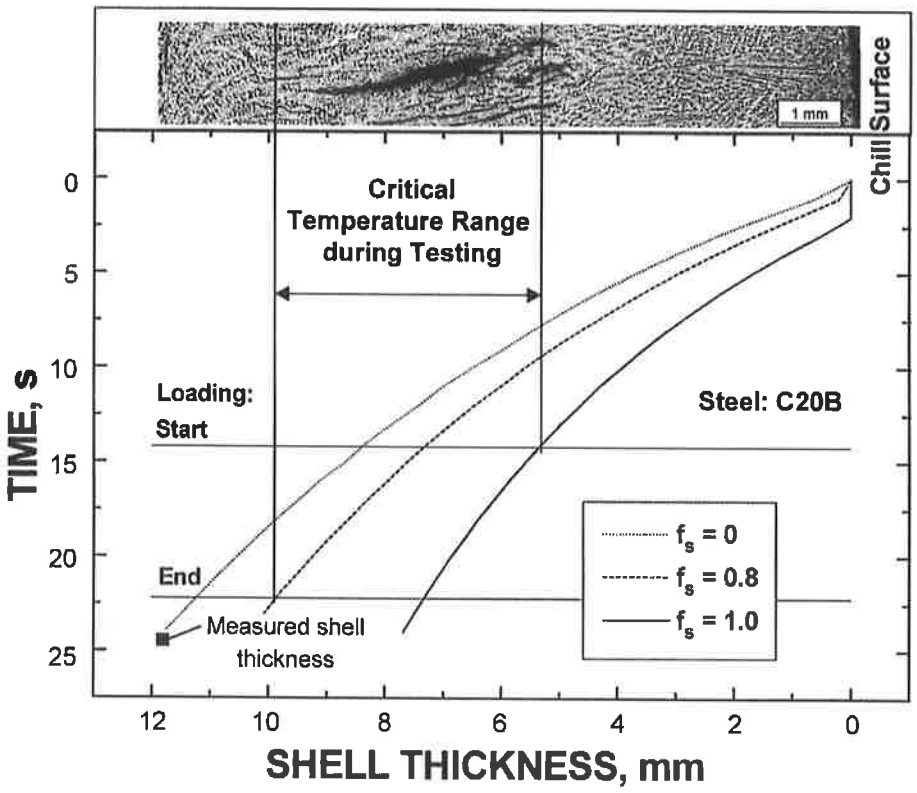

Fig. 9 – Microsection with interdendritic crack and shell growth derived from thermal analysis during SSCT test for steel C20B.

Fig. 9 – Section métallographique avec crique interdendritique et croissance de peau calculée à partir de l'analyse thermique pendent l'essai SSCT pour acier C20B.

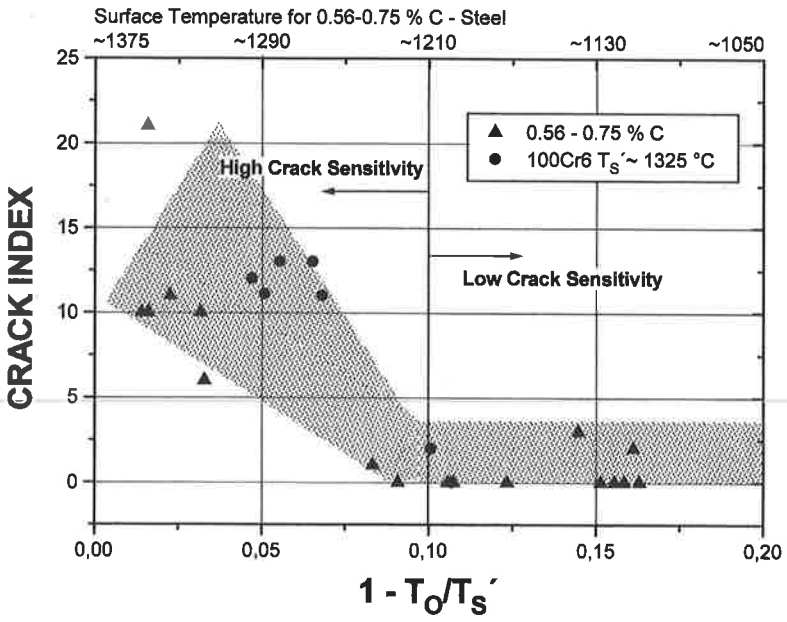

Fig. 10 – Inner crack index versus homologous temperature and shell surface temperature in the SSCT test for C60 and 100Cr6 steels.

Fig. 10 – Indice de criques internes en relation avec la température homologue et la température en surface de peau en essai SSCT pour aciers C60 et 100Cr6.

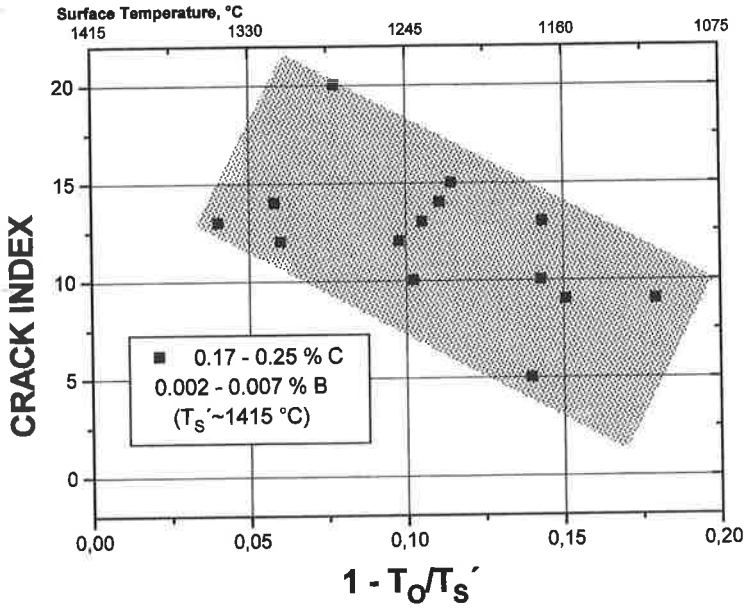

Fig. 11 – Inner crack index versus homologous temperature and shell surface temperature in the SSCT test for C20B steels.

Fig. 11 – Indice de criques internes en relation avec la température homologue et la température en surface de peau en essai SSCT pour aciers C20B.

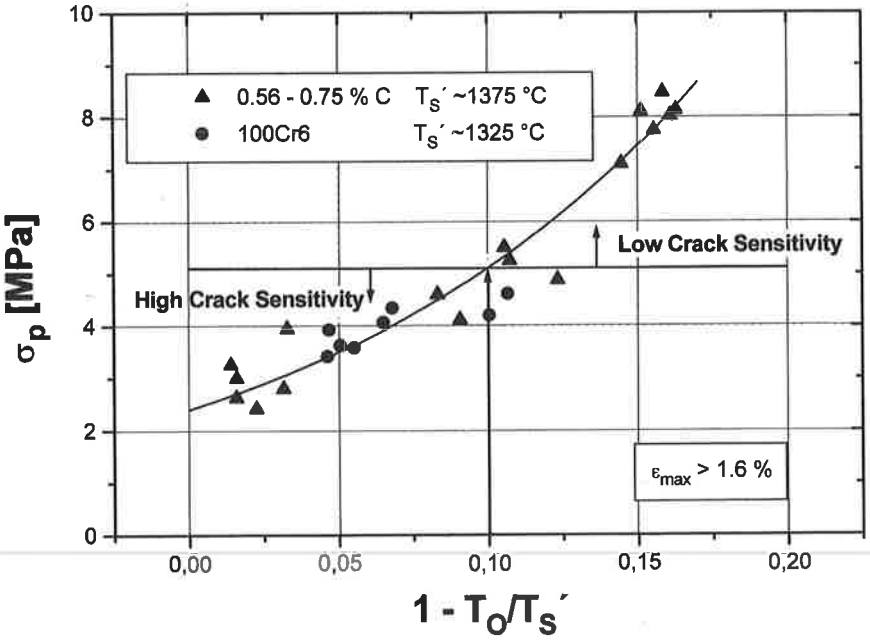

Fig. 12 – Maximum shell strength of high C steels measured in the SSCT test versus homologous temperature.

Fig. 12 – Résistance maximale de peau pour aciers à haut carbone mesurée en essai SSCT en relation avec la température homologue.

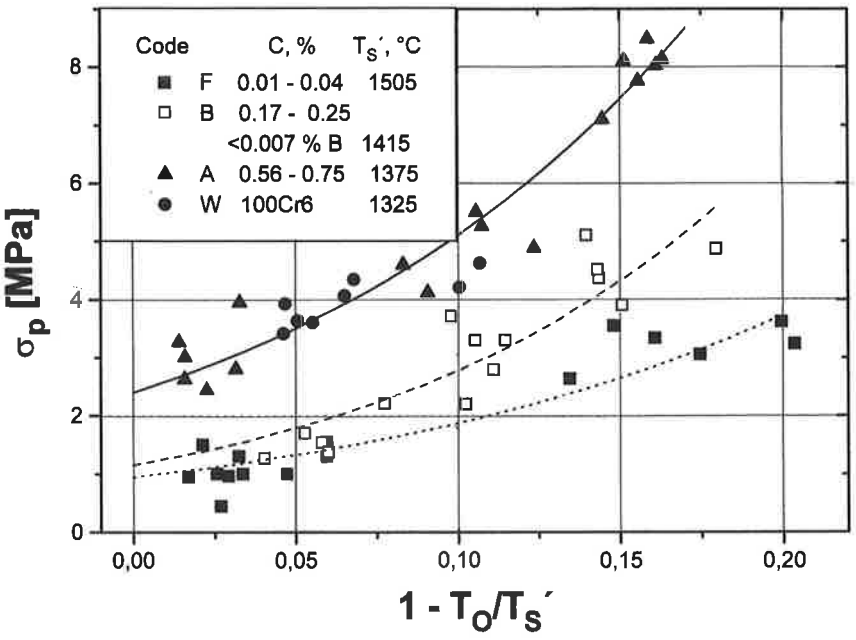

Fig. 13 – Maximum shell strength measured in the SSCT test versus homologous temperature for four steel groups.

Fig. 13 – Résistance maximale de peau mesurée en essai SSCT en relation avec la température homologue pour quatre groupes d'aciers.

The tests for low C steels of type C02 (not shown here) revealed interdendritic cracking only for samples close to solidus temperature, i.e. a homologous temperature $T_0/T_S' > 0.93$.

■ DISCUSSION

Aspects concerning the cracking mechanism

These results point to a rather clear limit of shell strength for high C steels around 5 MPa *(fig. 12)*. Such deformation limit could be attributed to the transition from visco-elasto-plastic to a mainly elastoplastic flow behaviour at the lower shell surface temperature, which prevents local strain concentration between interdendritic stices (12), in favour of uniform strain distribution over the charged sample length.

However, this argument might even more apply to the much softer ferritic matrix of the C02 steels. Nevertheless, their reduced cracking tendency (critical stress below 2 MPa, *fig. 13*), points to a different crack mechanism : accounting for the large difference in microsegregation sensitivity between the ferritic and austenitic matrix, rather the extent of interdendritic and intergranular precipitates seems to be the overruling factor in crack susceptibility. Such factor also renders aspects of morphology, i.e. cellular dendritic growth of low C steels versus extensive side arm branching of high C steels, negligible with respect to interdendritic decohesion.

Nevertheless, the measured data obtained from the SSCT test can now provide a much more accurate basis to develop a stress criterion for inner cracking (17). This has already been attempted previously, e.g. (18 to 22), but based on inadequate strength data which were derived from classical hot tensile tests that cannot simulate CC conditions as closely as the SSCT test.

Aspects of process control

To avoid excessive straining of the tiny meniscus shell, tensile ("drag") force exerted by mould friction is usually relieved during the negative strip period. Interfacial shear stress due to strand/mould friction is much lower than the shell matrix strength (23). But casting with only positive strip appears to lead invariably to sticker breakouts (24). At least a "stop-go" withdrawal rythm is required as realized in horizontal continuous casting (HCC), for instance. It could be of interest to include in future SSCT simulation trials such intermittent withdrawal to check its effect on stress-strain behaviour and interdendritic cracking.

As already outlined in the introduction, a correct mould taper represents the key requirement for cooling rate control during initial solidification. Since the course of

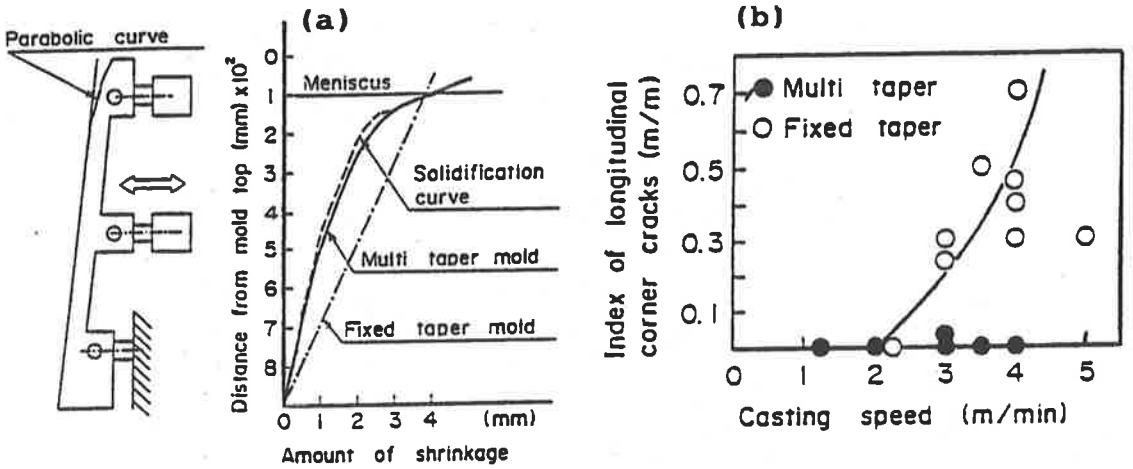

Fig. 14 – Effect of mould taper on longitudinal corner cracking (a) and on achievable casting speed (b) (C06, 90 × 1000 mm²) (26).

Fig. 14 – Effet de la conicité de lingotière sur les criques longitudinales (a) et sur la vitesse de coulée utilisable pour des brames (b) (C06, 90 × 1000 mm²) (26).

shell surface temperature below the meniscus is not linear (e.g. *fig. 4*), a stronger taper is required initially, mostly assuming a parabolical profile, and very successful applications of such a design are reported in the literature e.g. (25 to 27) *(fig. 14)*. The ultimate process control uses on-line monitoring of local heat transfer by thermocouples embedded in the mould wall at strategic positions :

– the example in *figure 15* illustrates the detection of transverse depressions in bloom casting (28) ;

– detection of longitudinal depressions is exemplified for stainless steel slabs in *figure 16* (29) ;

– an arrangement of thermocouples in the off-corner position of slab mould NF apt to detect any depression formation there *(fig. 17)* (30).

Corresponding heat flow modelling can convert such local loss in heat flux into the respective rise in shell surface temperature (11).

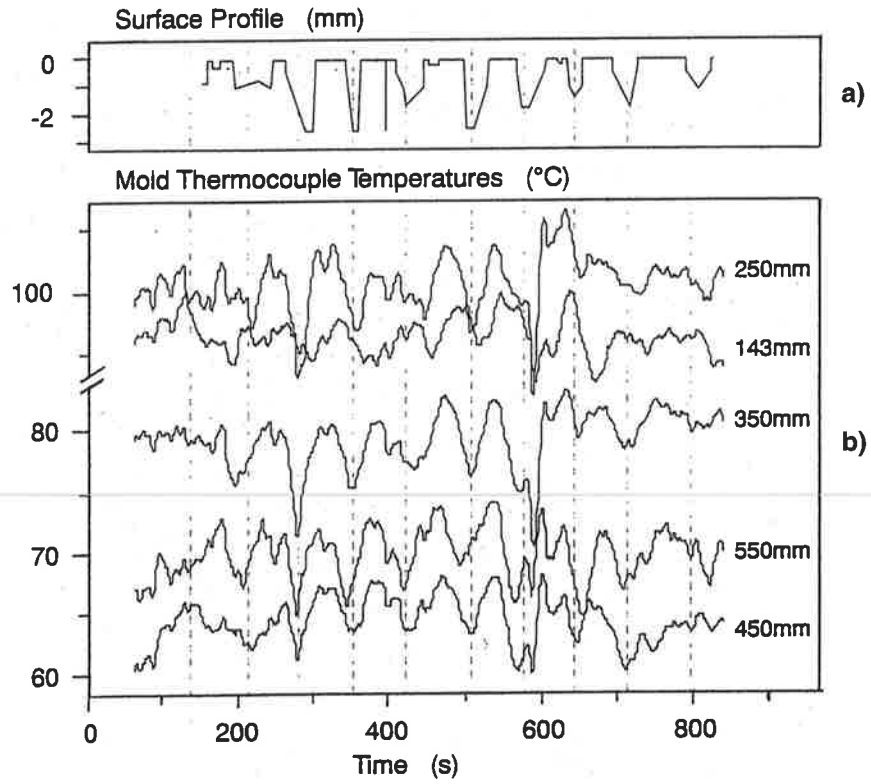

Fig. 15 – Longitudinal profile of bloom surface geometry and course of mould wall temperature over time (C06, 400 × 630 mm², 0.5 m/min) (28).

Fig. 15 – Profil longitudinal de la géométrie de surface des blooms et évolution de la température en paroi de lingotière avec le temps (C06, 400 × 630 mm², 0,5 m/min) (28).

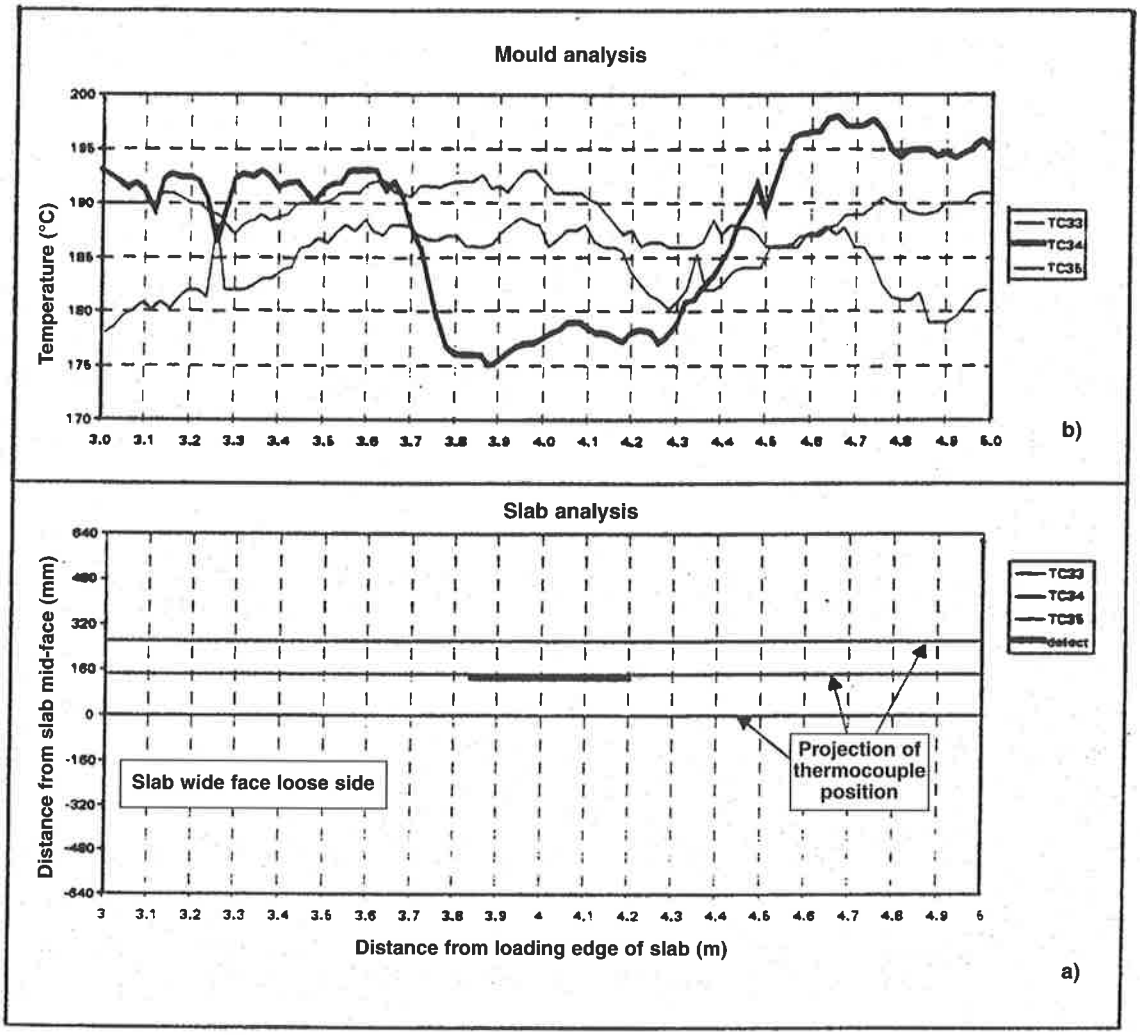

Fig. 16 – Course of mould wall temperature (a) and slab surface report for longitudinal mid-face depression (b) for 304 stainless steel (210 × 1200 mm², 1.0 m/min) (29).

Fig. 16 – Évolution de la température en paroi de lingotière (a) et indicateur de la présence de dépressions à mi-face à la surface de brames (b) pour acier 304 (210 × 1200 mm², 1,0 m/min) (29).

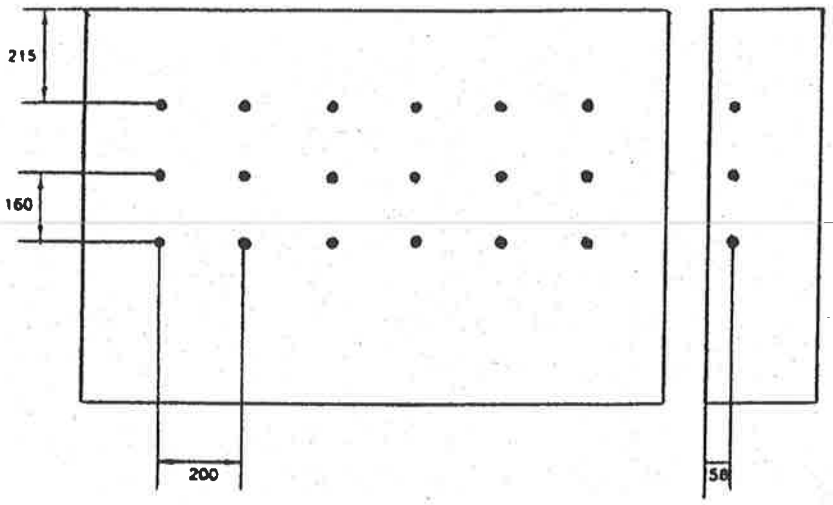

Fig. 17 – Position of thermocouples for local heat flux monitoring in C steel slab casting (30).

Fig. 17 – Position des thermocouples pour la mesure du flux thermique local en coulée continue de brames en aciers au carbone (30).

■ CONCLUSION

• Subsurface crack formation in CC strands, harmful to product quality and operational safety alike, is related to locally reduced heat transfer, causing a hot spot which weakens shell strength.

• The experimental values of shell strength derived in the new SSCT test method and corresponding observations on inner crack occurrence allow to define approximate critical limits in terms of shell strength and strand surface temperature required for crack-free shell formation.

• These limits can be applied to on-line heat transfer monitoring by thermocouples to assess the likelihood of crack formation connected with surface depressions, in order to activate process control accordingly (casting speed and mould taper optimisation, lubricant selection and application, choice of oscillation parameters, etc.).

■ REFERENCES

(1) WOLF (M.M.). Steelmaking Conference Proceedings, ISS, 82 (1999), p. 3.

(2) REGE (J.S.), HUA (M.), GARCIA (C.I.), DE ARDO (A.J.). 38th MWSP Conference Proceedings, ISS, 34 (1997), p. 555.

(3) NEUTJENS (J.), MATHY (H.), HERMAN (J.C.). *La Revue de Métallurgie-CIT*, n° 4 (1997), p. 551.

(4) LI (D.-M.), HESSLING (G.), BLECK (W.). *Steel Research*, 70, n° 4/5 (1999), p. 154.

(5) WINTZ (M.), BOBADILLA (M.), JOLIVET (J.M.). *La Revue de Métallurgie-CIT*, n° 1 (1994), p. 105.

(6) JAUCH (R.), LÖWENKAMP (H.), REGNITTER (F.), FISCHER (K.), SCHROER (H.), SIMON (R.W.), JERICHO (E.). *Metallurgical Plant and Technology*, n° 2 (1978), p. 24.

(7) BRIMACOMBE (J.K.), HAWBOLT (E.B.), WEINBERG (F.). *Canadian Metallurgical Quarterly*, 19 (1980), p. 215.

(8) BOMMARAJU (R.), BRIMACOMBE (J.K.), SAMARASEKERA (I.V.). *ISS Transactions*, 5 (1984), p. 95.

(9) DIPPENAAR (R.J.), SAMARASEKERA (I.V.), BRIMACOMBE (J.K.). *ISS Transactions*, 7 (1986), p. 31.

(10) GRILL (A.), SORIMACHI (K.), BRIMACOMBE (J.K.). *Metallurgical Transactions B*, 7B (1976), p. 177.

(11) LAWSON (G.D.), SANDER (S.C.), EMLING (W.H.), MOITRA (A.), THOMAS (B.G.). Steelmaking Conference Proceedings, ISS, 77 (1994), p. 329.

(12) BERNHARD (C.), HIEBLER (H.), WOLF (M.M.). *ISIJ International*, 36 (1996), Supplement, p. S163.

(13) BERNHARD (C.). Mechanical properties and crack susceptibility of solidifying steel under continuous casting conditions. Doctor-thesis, Montanuniversität Leoben (1998).

(14) HIEBLER (H.), BERNHARD (C.). *Steel Research*, 70 (1999), p. 349.

(15) OHNAKA (I.). *Transactions ISIJ*, 26 (1986), p. 1045.

(16) YAMANAKA (A.), NAKAJIMA (K.), YASUMOTO (K.), KAWASHIMA (H.), NAKAI (K.). *La Revue de Métallurgie-CIT*, n° 7/8 (1992), p. 627.

(17) HIEBLER (H.), ZIRNGAST (J.), BERNHARD (C.), WOLF (M.M.). Steelmaking Conference Proceedings, ISS, 77 (1994), p. 405.

(18) GRILL (A.), BRIMACOMBE (J.K.), WEINBERG (F.). *Ironmaking and Steelmaking*, 3 (1976), p. 38.

(19) SORIMACHI (K.), BRIMACOMBE (J.K.). *Ironmaking and Steelmaking*, 4 (1977), p. 240.

(20) CORNELISSEN (M.C.M.). Steelmaking Conference Proceedings, ISS, 69 (1986), p. 357.

(21) RAMACCIOTTI (A.). *Steel Research*, 59 (1988), p. 438.

(22) REZA ABOUTALEBI (M.), HASAN (M.), GUTHRIE (R.I.L.). *Steel Research*, 65 (1994), p. 225.

(23) WOLF (M.). Steelmaking Conference Proceedings, 74 (1991), p. 51.

(24) FOERSTER (E.), GUDENAU (H.W.), KEMPER (G.M.), STERCKEN (K.). *Stahl und Eisen*, 113, n° 9 (1993), p. 93.

(25) FUJIYAMA (T.), MIYAGAWA (S.), DESHIMARU (S.), MIZOTA (H.). Steelmaking Conference Proceedings, ISS, 68 (1985), p. 215.

(26) MURAKAMI (T.), YAMADA (T.), OKAMURA (K.), HASHIO (M.), KAWAKAMI (T.), WATANABE (T.). *CAMP-ISIJ*, 5, n° 4 (1992), p. 1291.

(27) HORBACH (U.), KOCKENTIEDT (J.), JUNG (W.). *Stahl und Eisen*, 117, n° 12 (1997), p. 95.

(28) JENKINS (M.), THOMAS (B.G.), CHEN (W.C.), MAHAPATRA (R.B.). Steelmaking Conference Proceedings, ISS, 77 (1994), p. 337.

(29) BELLOMO (P.), BRASCUGLI (G.), MILONE (M.), SPACCAROTELLA (A.), SANARICO (M.), VICINO (F.). Steelmaking Conference Proceedings, ISS, 81 (1998), p. 199.

(30) BELLOMO (P.), SALVEMINI (G.), SANTA MARIA (E.), VICINO (F.). Steelmaking Conference Proceedings, ISS, 77 (1994), p. 319.

Christian BERNHARD, 33 years, Dipl.-Ing. and Dr. mont., university assistant at Institute of Ferrous Metallurgy, Montanuniversität Leoben, Austria, since 1998.

Herbert HIEBLER, 64 years, Dipl.-Ing. and Dr. mont, university professor at Institute of Ferrous Metallurgy, Montanuniversität Leoben, Austria, since 1979.

Manfred M. WOLF, 62 years, Dipl.-Ing. and Dr. sc. techn. ETH, independent consultant in continuous casting under Wolftechnology since 1988, and extramural lecturer in "Continuous Casting" at Institute of Ferrous Metallurgy, Montanuniversität Leoben, Austria, since 1990.